JMEPEG (2022) 31:10213–10224
https://doi.org/10.1007/s11665-022-07029-3

1059-9495/$19.00

TECHNICAL ARTICLE

Effect of Mo-Related Precipitation Behavior on the Strengthening and Thermal Stability of 4Cr5Mo2V Die Steel

Tao Hu, Riming Wu, Fangjie Li, Na Min, and Wei Li

Submitted: 2 December 2021 / Revised: 29 April 2022 / Accepted: 10 May 2022 / Published online: 23 June 2022

The effect of molybdenum content (1.25, 2.25, 3.0 wt.%) on the microstructure, mechanical properties, and thermal stability of 4Cr5Mo2V steel has been investigated. The increase of Mo content promotes the transition of $M_{23}C_6$ to M_6C and inhibits the nucleation and growth of $M_{23}C_6$, as supported by the transmission electron microscope observation presented in this paper. The result shows that the mechanical properties and the thermal stability at 620 °C are both strongly dependent on the Mo content. The yield/tensile strengths at room temperature of 1.25, 2.25, and 3.0% Mo steels are 1028/1287, 1080/1347, and 1114/1402 MPa; meanwhile, the elongation is 23, 26, and 27%, respectively. And the yield/tensile strengths at 620 °C of the 1.25, 2.25, and 3.0% Mo steels are 285/661, 379/714 and 335/690 MPa; meanwhile, the elongation is 23, 20, and 22%, respectively. The M_6C-type nano-carbides in the three steels enhance the tensile strength through the Orowan bypass strengthening mechanism, providing increments of tensile strength of 145 MPa (1.25 Mo), 167 MPa (2.25 Mo), and 182 MPa (3.0 Mo), respectively. It is obvious that the coarsening kinetics of solute atoms in three steels is controlled by volume diffusion during the tempering at 620 °C. The Avrami exponent n of the 1.25, 2.25, and 3.0% Mo steels at 620 °C is 0.42, 0.41, and 0.37, respectively. The calculations were in consistent with the finding that the average precipitation rate and coarsening rate of carbides in 3.0 Mo steel are the lowest.

Keywords 4Cr5Mo2V, mechanical properties, microstructure, molybdenum, thermal stability

1. Introduction

Hot work die steels are widely used in hot forging, hot extrusion and die casting dies (Ref 1, 2). Among them, 4Cr5Mo2V steel is an ideal Cr-Mo-V hot working die material, which is widely used in hot forging and die casting industry because of its excellent heat resistance and thermal fatigue performance (Ref 3). With the rapid development of the mold industry, high quality die and mold with large-scale, high precision of dimensions, complex cavity as well as long lifetime are required. As the working temperature of hot work die steel reached about 500-700 °C (Ref 4, 5), the microstructure continued to deteriorate, and the hardness declined (Ref 6-8). The softening phenomenon is mainly manifested by the decrease of hardness and high temperature strength, owing to the gradual coarsening and the growth of fine carbides at high temperature and the decrease of dislocation density (Ref 5, 9, 10). The simultaneous loss of hardness and high temperature strength would lead to accidental die failure, which greatly shortens the service life of the die (Ref 11).

Researchers have conducted studies on adjusting alloying composition to tailor the microstructure, the precipitation of secondary carbides, and the resulting performance (Ref 12-16). Cr can participate in the form of nanoscale MC carbides and M_2C carbides (Ref 17), providing a strengthening effect. However, Cr tends to form carbides with large volume and low toughness (Ref 18). V is the main component of MC nano-carbides, which can improve the thermal stability and high temperature performance by nano-carbides (Ref 19-21). Mo can not only enhance the room temperature strength of steels by precipitating the separation of fine MC and M_2C carbides, but it also improves the high temperature yield strength of steels with the nanoscale carbides (Ref 22, 23). Researches showed molybdenum tended to be distributed in the outer region of the precipitated phase by replacing the M atoms (V, W, Cr, and Fe) (Ref 24). The concentration of molybdenum in niobium-rich carbide precipitations was also proved by Lee et al. Ref 14 to enhance high-temperature strength by uniform distribution of fine MC particles (Ref 25). However, excessive carbide forming elements would lead to carbide coarsening, and brittleness of steel.

However, despite all the previous studies, the optimum alloying element range is urgent to be revealed for hot work die steels, especially for the role of Mo in the precipitation process. Therefore, in this work, 4Cr5Mo2V steels with different Mo contents (1.25, 2.25, 3.0 wt.%) were prepared. The strengthening mechanism and Mo-related precipitation behavior were systematically studied.

Tao Hu, Riming Wu, and **Fangjie Li**, School of Material Engineering, Shanghai University of Engineering Science, Shanghai 201600, China; **Na Min**, Key Laboratory for Microstructures, Shanghai University, Shanghai 201600, China; and **Wei Li**, School of Materials Science and Engineering, Shanghai JiaoTong University, 800 Dongchuan Rd, Shanghai 200240, China. Contact e-mail: 05170001@sues.edu.cn.

2. Materials and Experimental Methods

2.1 Materials

The nominal chemical compositions (wt.%) of the test alloy samples are listed in Table 1. The test alloys were designed with different Mo contents to investigate the strengthening and thermal stable mechanism of the steels. An ingot of 20 kg per branch was prepared by vacuum induction melting. Three-dimensional forging was applied after homogenization at 1240 °C for 5 h, to produce steel plates with a size of 28 × 60 × 800 mm, followed by spheroidizing annealing treatment. The Ac3, Ac1 and Ms temperatures of 1.25%Mo steel measured by dilatometry were 868, 840, and 263 °C, respectively. The Ac3, Ac1 and Ms temperatures of 2.25% Mo steel measured by dilatometry were 858, 832, and 270 °C, respectively. The Ac3, Ac1 and Ms temperatures of 3.0% Mo steel measured by dilatometry were 866, 830, and 275 °C, respectively (Fig. 1). So the 1030 °C was determined as the normalization temperature to dissolve all the carbides in test steels.

2.2 Microstructure Observation

Scanning electron microscopy (SEM) observation was carried out by Tescan VEGA3 SEM with an accelerating voltage of 10.0 kV equipped with an Oxford energy dispersive spectroscopy (EDS) system. Transmission electron microscopy (TEM) specimens were examined by JEOL TEM operated at 200 kV in conjunction. Disks with size of Ø3 mm × 60 μm specimens for TEM observation were prepared by double jet electrolytic polishing. Scanning transmission electron microscope (STEM) with energy dispersion spectrometer (EDS) was conducted on Ø3 mm × 30 μm after double-spray electrolytic thinning by 7 vol.% perchloric alcohol solution. STEM observation was carried out in a JSM-6700F microscope operated at 300 kV.

2.3 Mechanical Property

Standard tensile specimens with a gage diameter of 5 mm and a gage length of 25 mm were machined. A Zwick tensile tester (Model TN.A50) was employed for tensile testing with a strain rate of 0.003 s^{-1}. Three specimens were tested at room temperature 25 °C and the average values were recorded.

2.4 Thermal Stability

The 1.25, 2.25, and 3.0% Mo steel specimens with the size of 20 × 30 × 50 mm were austenitized for 1 h at 1030 °C, and quenched in oil to room temperature. The quenched specimens of 1.25, 2.25, and 3.0% Mo steels were subsequently tempered for 2 h at 600, 605 and 620 °C, respectively. A similar hardness of 47 HRC was reached in all of the specimens. The specimens were additionally tempered for different period at 620 °C.

Table 1 The nominal chemical compositions (wt.%) of samples

Elements alloys with different contents of Mo	C	Si	Mn	Cr	Mo	V	Fe
1.25% Mo	0.41	0.38	0.55	5.00	1.25	0.55	Bal.
2.25% Mo	0.41	0.38	0.55	5.00	1.25	0.55	Bal.
3.0% Mo	0.41	0.38	0.55	5.00	3.0	0.55	Bal.

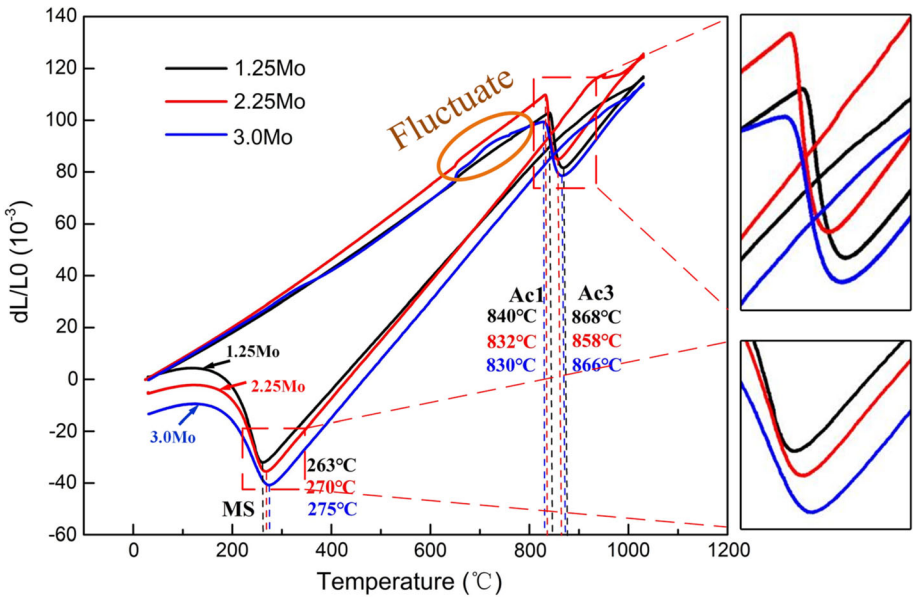

Fig. 1 Thermal dilatometry curves of experimental steels during slow heating to 1030 °C and fast cooling to ambient temperature

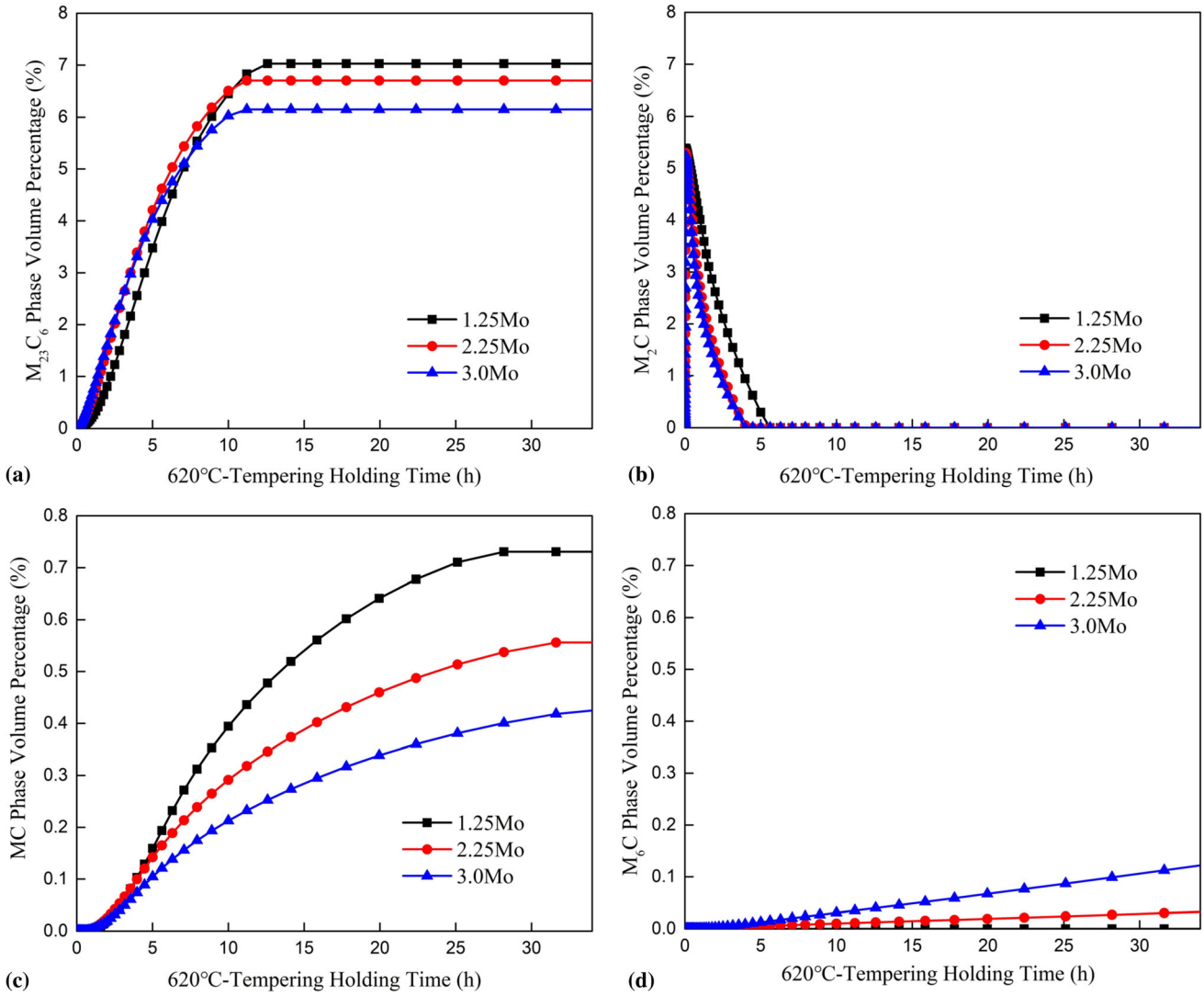

Fig. 2 The evolution of carbides simulated by JMatPro in quenched experimental steels with different Mo contents when tempering at 620 °C, (a) $M_{23}C_6$, (b) M_2C, (c) MC, and (d) M_6C

3. Results

3.1 Prediction of Precipitation

JMatPro software was applied to predict the evaluation of carbides in quenched and tempered experimental steels. Figure 2 exhibits the evaluations of equilibrium volume fraction of $M_{23}C_6$ (a), M_2C (b), MC (c), and M_6C (d) carbides, respectively. Tempered at 620 °C, the mass fraction of $M_{23}C_6$ (Fig. 2a) gradually decreases with the increase of Mo content. Because the $M_{23}C_6$ carbide growth rate was relatively high (Ref 10), it was not conducive to improving the tempering stability of die steel. The formation of $M_{23}C_6$ was inhibited. The mass fraction of M_2C (Fig. 2b) carbides gradually decreases with the increase of tempering time. At the same holding time in tempering, with the increases of Mo content, the amounts of MC and M_2C (Fig. 2b and c) carbides gradually decreased. It could be attributed to the fact that the vacancy of M positions in MC carbides was occupied by Mo (Ref 19-21), then tend to transition to M_6C carbide. Mo was also observed to promote the formation M_6C carbides in Fig. 2(d).

3.2 Mechanical Properties

The tensile curves of experimental steels with different Mo contents at room temperature are shown in Fig. 3 with Mo content increasing from 1.25 to 3.0%, the tensile strength linearly increasing from 1287 to 1402 MPa, and the yield strength increasing from 1028 to 1114 MPa, while the total elongation decreased from 27 to 23%.

Figure 4 exhibits the tensile properties of samples with different Mo content at 620 °C. With the content of Mo increasing from 1.25 to 2.25%, the tensile strength from 661 to 714 MPa, and the yield strength from 285 to 379 MPa, while the total elongation decreased from 20 to 23%. However, the content of Mo increasing from 2.25 to 3.0%, the tensile strength decreased from 714 to 690 MPa, and the yield strength decreased from 379 to 335 MPa, while the total elongation increased from 20 to 22%.

Figure 5 shows the Rockwell hardness curves for the 1.25, 2.25 and 3.0% Mo steels as a function of tempering time at 620 °C. As holding time prolonged, the hardness values of three steels decrease, and the slopes of the hardness curves became gradually stable. According to Fig. 5, the initial

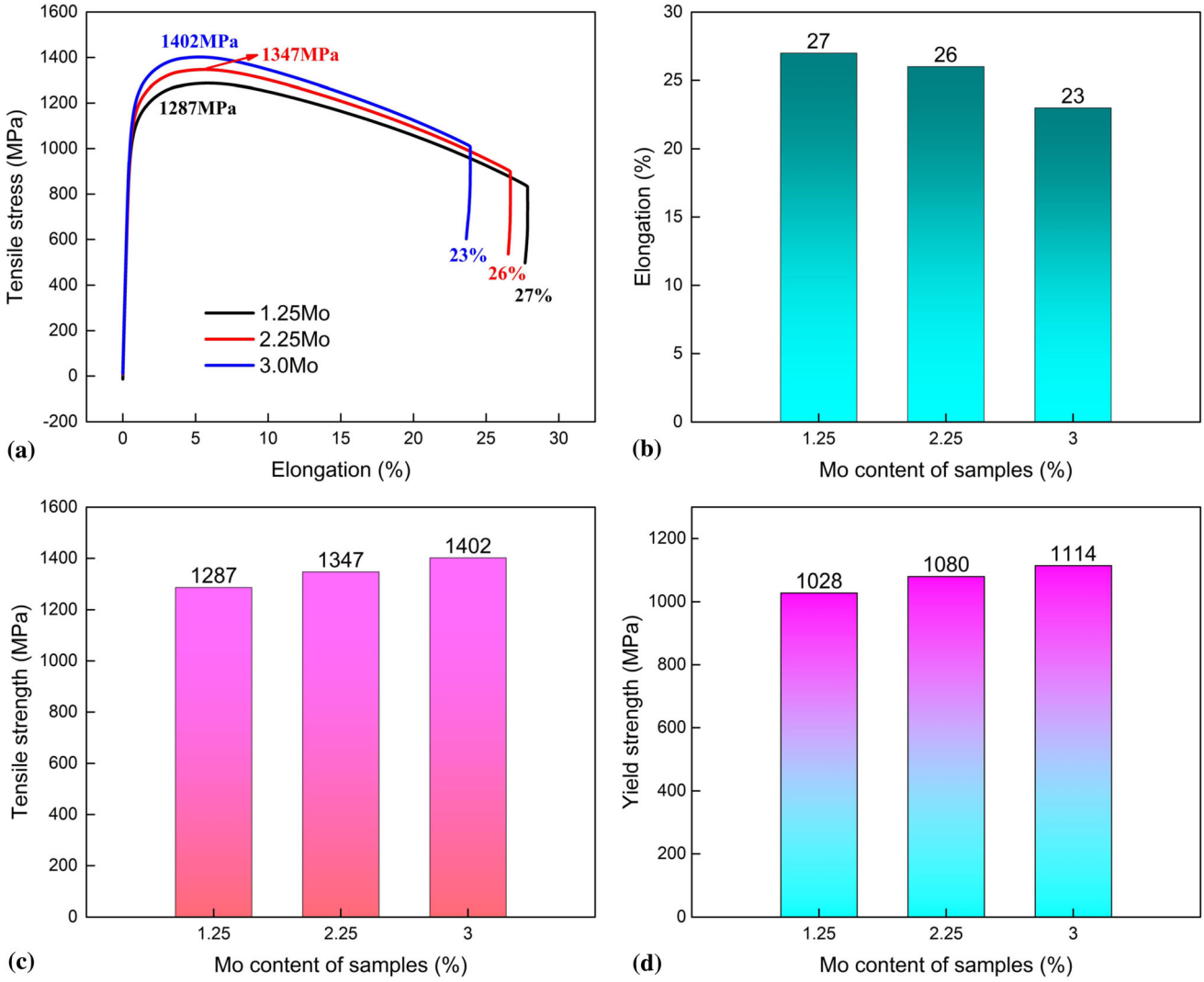

Fig. 3 Tensile properties of the specimens quenched at 1030 °C and tempered at 620 °C, (a) tensile curves, (b) elongation at room temperature, (c) Tensile strength at room temperature, and (d) yield strength at room temperature

hardness values of the quenched and tempered 1.25, 2.25 and 3.0% Mo steels were 46.7, 46.8 and 47.0 HRC, respectively. After 10 h holding at 620 °C, the hardness of the three tested steels decreased to 34.0, 36.0 and 38.0 HRC, respectively. The hardness of the three tested steels finally decreased to 28.4, 30.0 and 31.8 HRC, respectively, after 34 h of tempering at 620 °C.

3.3 Microstructure Observation

Figure 6 exhibits the SEM images of the experimental steels tempered at 620 °C for 2, 10, and 24 h, respectively. It can be observed that rod-like and spherical carbides appeared in the microstructures of three steels. After being held at 620 °C for 10 h, the rod-like carbides in the three test steels disappeared and only the spherical carbides were found, while the spherical carbides grew up to a certain extent. Finally, the spherical carbides coarsened obviously at 620 °C after 24 h of tempering, and the coarsening phenomenon became more obvious with the increase of Mo content.

Figure 7 shows the XRD patterns of the three test steels after being tempered at 620 °C for 10 h. Apparently, no retained austenite was observed in the test steels, and the volume fraction of the residual austenite in the test steels was below the detection limit (usually below 3 vol.% (Ref 26)), whereas only α (martensite) peaks can be seen in all tested steels.

Figure 8 shows the size distribution of M_6C nano-carbides in the specimens with different Mo contents. It was deduced from the diffraction patterns that the short rod carbides were M_6C type carbides, and the large irregular granular carbides were $M_{23}C_6$ type carbides as shown in (Fig. 8c, f and i). The average lengths and widths of nano-carbides were obtained by ImageJ software. It can be seen that the average length of M_6C nano-carbides in the 1.25, 2.25, and 3.0% steels was 65 ± 1, 78 ± 1 and 50 ± 1 nm, and the average diameter was 20 ± 1, 24 ± 1, and 18 ± 1 nm, respectively. Moreover, Mo enrichment phenomenon was found in $M_{23}C_6$ carbide as proved by EDS data in Table 3.

Figure 9 shows the STEM-EDS data of carbides in 1.25 Mo steel tempered at 620 °C for 10 h. There were two types of carbides in 1.25%Mo steel, among which one was rod shape and the other was small spherical. The sizes of carbides as shown in Fig. 8(a) ranged from 15 to 40 nm. There were four selected points in Fig. 9(a) (point EDS1, EDS2, EDS3, and

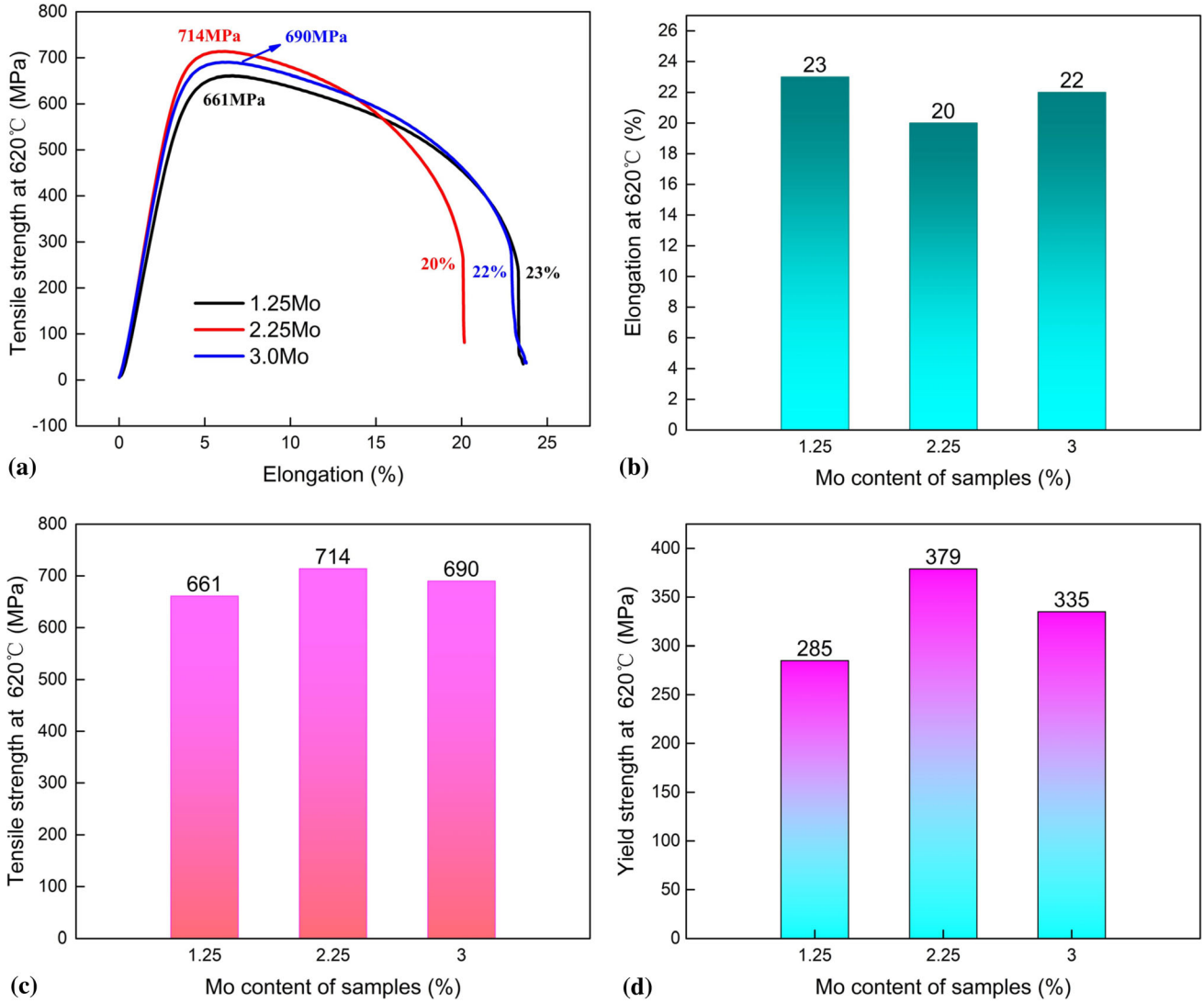

Fig. 4 Tensile properties of the specimens quenched at 1030 °C and tempered at 620 °C with different Mo content at 620 °C, (a) tensile curves, (b) elongation at 620 °C, (c) Tensile strength at 620 °C, and (d) yield strength at 620 °C

EDS4) to detect the alloy compositions. The detailed compositions in atomic percent and atomic ratios of Cr, Mo, V, Mn, and Fe are shown in Table 2. It should be noted that the deviations of carbon content were relatively larger, so carbon and ferrite contents of each point were discarded. The average atomic ratios of Cr/Mo, Cr/V, Cr/Fe, Mo/V, Mo/Fe, and V/Fe varied from one carbide to another. The fluctuations of atomic percentages mostly relied on the measurement accuracy of STEM-EDS equipment.

There were two kinds of carbides in 3.0 Mo steel tempered at 620 °C for 10 h as shown in Fig. 10(a), with one in rod shape and the other in large irregular granular shape. Six points in Fig. 10(a) (point EDS1, EDS2, EDS3, EDS4, EDS5, and EDS6) were selected to detect the alloy compositions. The detailed compositions in atomic percent and atomic ratios of Cr, Mo, V, Mn, and Fe, and the atomic ratios of Cr/Mo, Cr/V, Cr/Fe, Mo/V, Mo/Fe, and V/Fe are calculated in Table 3. It was found from Table 3 that the percentage of Mo in carbides with large irregular shape was obviously higher than the rod shape carbides. Because the error from detection of EDS was relatively bigger than XRD and TEM, 10 points (4 points in Table 2 and 6 points in Table 3) were selected for the analysis with the aim to avoid misjudgment on any element.

4. Discussions

4.1 Effect of Mo on Strength

The strengthening factor of die steels mainly includes solid solution strengthening, dislocation strengthening, grain refinement strengthening, and precipitation strengthening. The effects of solution strengthening and grain refinement strengthening of the three steels were almost the same during the long time tempering process (Ref 27). As shown in Fig. 5, an increase of Mo provides higher tensile strength and yield strength, but it exhibits a slight loss of elongation in 3.0% Mo steel. This may be related to the volume fraction and uniform dispersion of carbides in steel (Ref 13-16, 25). Study (Ref 22) had shown that the increase of Mo expanded the bainite transformation zone and increased the bainite volume fraction, leading to the effect of bainitic strengthening. Some studies (Ref 24, 28, 29) had

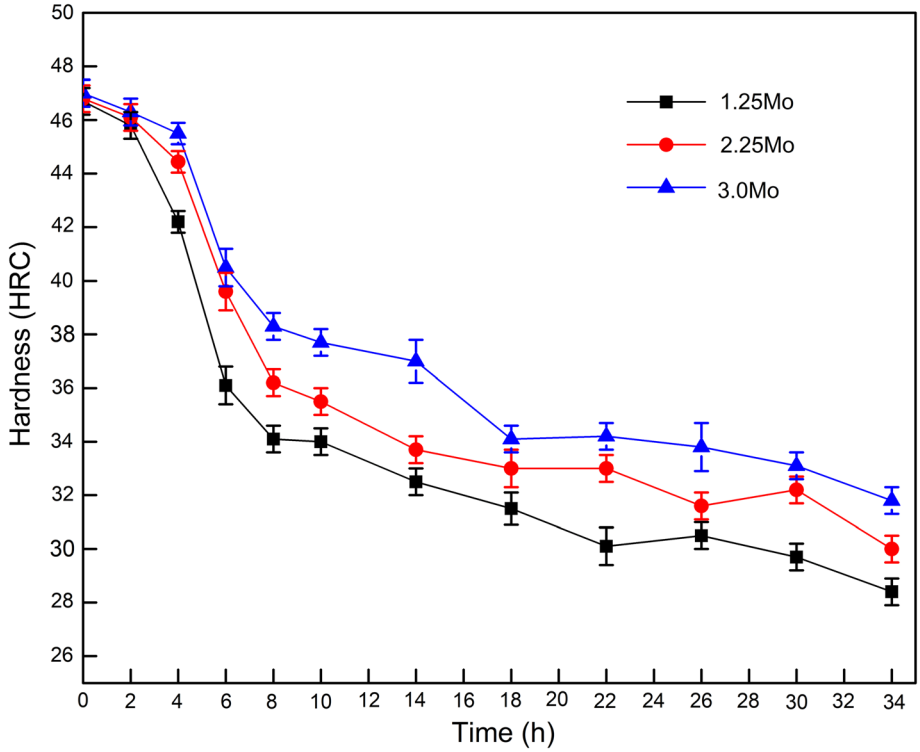

Fig. 5 Rockwell hardness as a function of tempering time at 620 °C for 1.25 Mo, 2.25 Mo, and 3.0 Mo steels

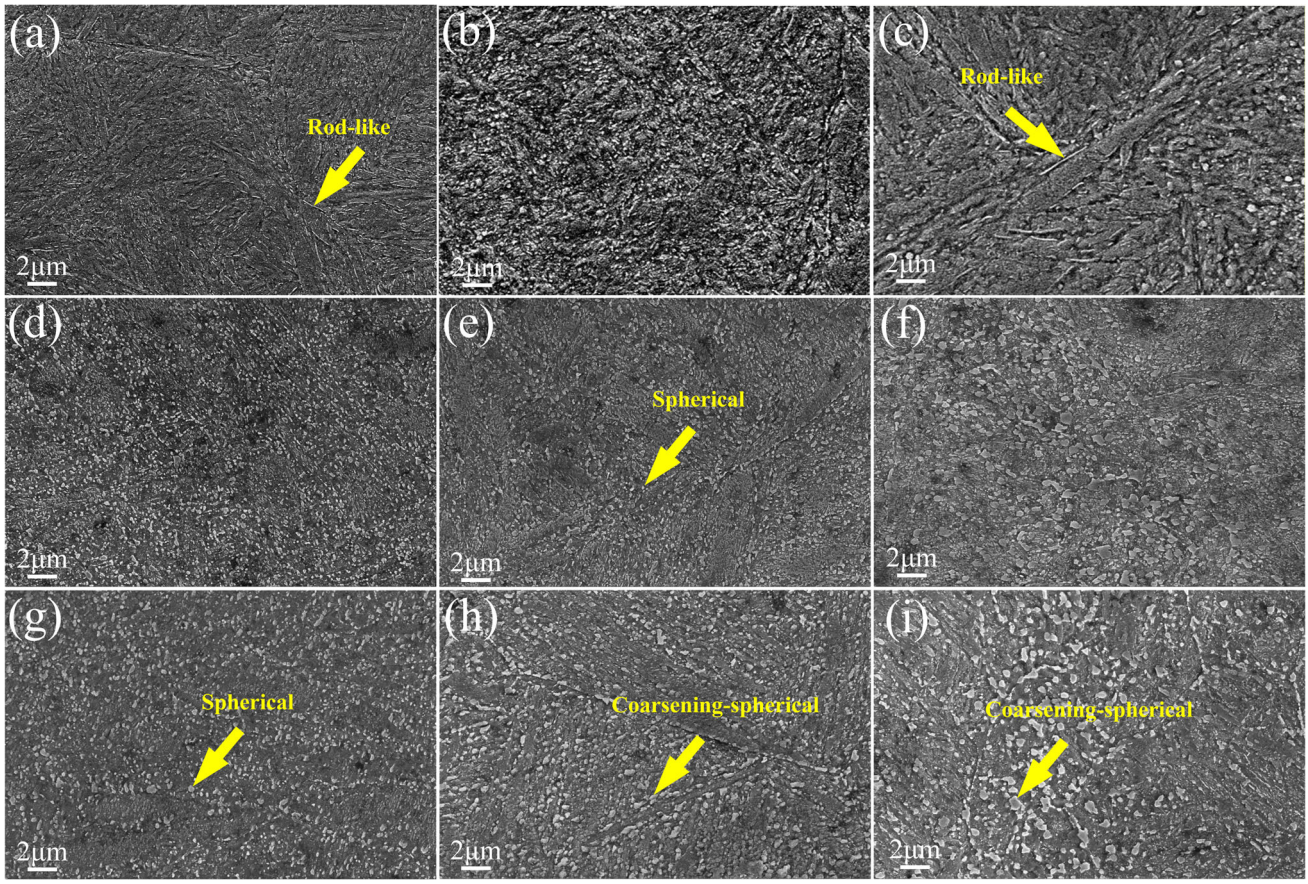

Fig. 6 SEM images of 1.25 Mo (a, d, g), 2.25 Mo (b, e, h), 3.0 Mo (c, f, i) steels by quenched and tempered treatment; (a, b, c) tempered at 620 °C for 2 h, (d, e, f) tempered at 620 °C for 10 h, (g, h, i) tempered at 620 °C for 24 h

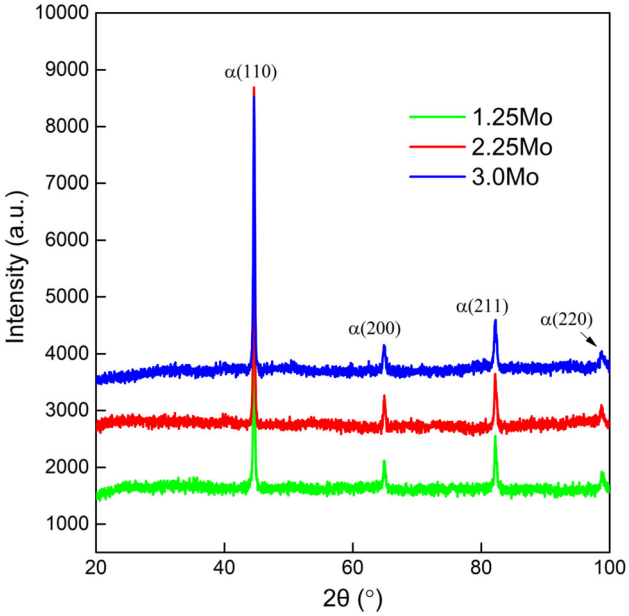

Fig. 7 XRD spectra of experimental quenched at 1030 °C and tempered at 620 °C for 10 h

also shown that Mo tends to form clusters to provide reinforcement. It can be proved in TEM images of both 2.25% Mo (Fig. 8d and e) and 3.0% Mo (Fig. 8g and h) steels. The effect of Mo on precipitation strengthening was obvious. The contribution of Mo related M_6C-type carbides to yield strength was calculated. The prediction results show that the rising of Mo content increase the volume fraction of M_6C. Thus, the pinning effect of carbide on dislocation is enhanced (Ref 30).

The precipitation strengthening effect of these carbides in experimental steels depends on the type of precipitates, average size, volume fraction and their interaction with dislocations (Ref 31). The strengthening of carbides is mainly achieved through shearing mechanism and Orowan bypass mechanism, which hinders the dislocation movement. The average equivalent diameters of precipitated phases of the three steels after 10h tempering at 620 °C were 33.91 ± 1, 40.69 ± 1, and 28.96 ± 1 nm, respectively, which were bigger than the critical size for Orowan looping of M_3C (10 nm) (Ref 32). Therefore, these precipitates were expected to be strengthened through the Orowan bypass mechanism. The improvement of yield strength based on shearing mechanism and Orowan bypass mechanism can be described as Eq 1 and 2, respectively [33].

$$\sigma_{\text{Shearing}} = \frac{2 \times 1.1}{\sqrt{2AG}} \times \frac{\gamma^{1/2}}{b^2} \times d_{\text{ae}}^{1/2} f^{1/2} \quad \text{(Eq 1)}$$

$$\sigma_{\text{Orowan}} = \frac{0.3728Gb}{K} \times \frac{f^{1/2}}{d_{\text{ae}}} \ln\left(\frac{1.2d_{\text{ae}}}{2b}\right) \quad \text{(Eq 2)}$$

$$A = \frac{1}{2\pi k} \ln\left(\frac{d_{\text{ae}}}{2b}\right) \quad \text{(Eq 3)}$$

where A is the dislocation tension function, which can be estimated by Eq 3; G is the shear elasticity modulus (80.65 GPa); γ is an average value of anti-phase boundary energy; b is the absolute value of the Burgers vector of dislocation (0.25 nm); K is the hybrid dislocation (0.83), can be estimated by $\frac{1}{K} = \frac{1}{2}\left(1 + \frac{1}{1-v}\right)$, where v is about 0.291; d_{ae} and f are the average equivalent diameters and the volume percentages of second-phase particles that are defined as Eq 4 and 5, respectively [33].

$$d_{\text{ae}} = \sqrt[3]{\frac{3}{2} l_a d_a^2} \quad \text{(Eq 4)}$$

$$f = \left(\frac{1.4\pi}{6}\right)\left(\frac{N d_{\text{ae}}^2}{S}\right) \quad \text{(Eq 5)}$$

where l_a is the average length; d_a is the diameter of the rod-shaped nano-carbides; S represents the area of photos in nm^2; N is the amounts of precipitates within a certain range.

The volume fraction of M_6C carbides was statistically counted on 8 TEM images ($2 \times 2\ \mu m^2$) of each steel. The parameters related to the calculation of nano-carbides strengthening are listed in Table 4. As shown in Table 4, the average equivalent size of the nano-carbides in the three steels exceeded the critical size (10 nm). The volume fractions of M_6C nano-carbides in the 1.25, 2.25, and 3.0% Mo steels are 1.53, 2.73, and 1.89%, respectively. Meanwhile, the M_6C nano-carbides in 1.25, 2.25, and 3.0% Mo steels contributed increments of 145, 167, and 182 MPa, respectively. As shown in Fig. 11, the calculated yield strength increase caused by the M_6C nano-carbides was consistent with the strength increments of the three steels.

The tensile strength and yield strength of the test steels at high temperature are much lower than those at room temperature, and the authors attribute this phenomenon to the thermal activation phenomenon at 620 °C, which makes dislocation slip and grain boundary slip more likely to occur (Ref 34). The decrease of dislocation density and interstice carbon concentration is accompanied by the dynamic recovery and recrystallization of matrix and the growth of carbide (Ref 35, 36). Because of the temper brittleness, the strength of the test steel decreases while the elongation decreases instead of increasing (Ref 37).

4.2 Effect of Mo on Thermal Stability

To evaluate the tempering stability of three steels, J-M-A equation was applied, $\tau = 1 - \exp(-(Dt)^n)$ [5], where τ is the tempering ratio, D is the temperature dependent diffusion coefficient, t is the tempering time, and n is the Avrami exponent, which depends on the material and the previous heat treatment. Tempering ratio τ is defined in $\tau = \frac{H - H_0}{H_\infty - H_0}$, where H_0, H_∞ and H are the hardness values of the quenched, annealed and the intermediate hardness at tempering ratio τ. The temperature dependent diffusion coefficient D is defined with $D = D_0 \exp\left(-\frac{Q}{RT}\right)$, where D_0 is the pre-exponential constant, Q is the activation energy of the tempering transformation, R is the ideal gas constant (8.13143 KJ mol^{-1} K^{-1}), and T is the isothermal tempering temperature in K. $s = 1 - \exp(-(Dt)^n)$ can be represented as a plot of $\ln\ln(1/(1-\tau))$ vs. $\ln t$, shown as Eq 6.

$$\ln\ln\frac{1}{1-\tau} = n \ln t + \ln D \quad \text{(Eq 6)}$$

The fitting results of Eq. 6 are shown in Fig. 12. Avrami exponent n of the 1.25, 2.25, and 3.0% Mo steels at 620 °C were 0.42, 0.41, and 0.37, respectively. According to the

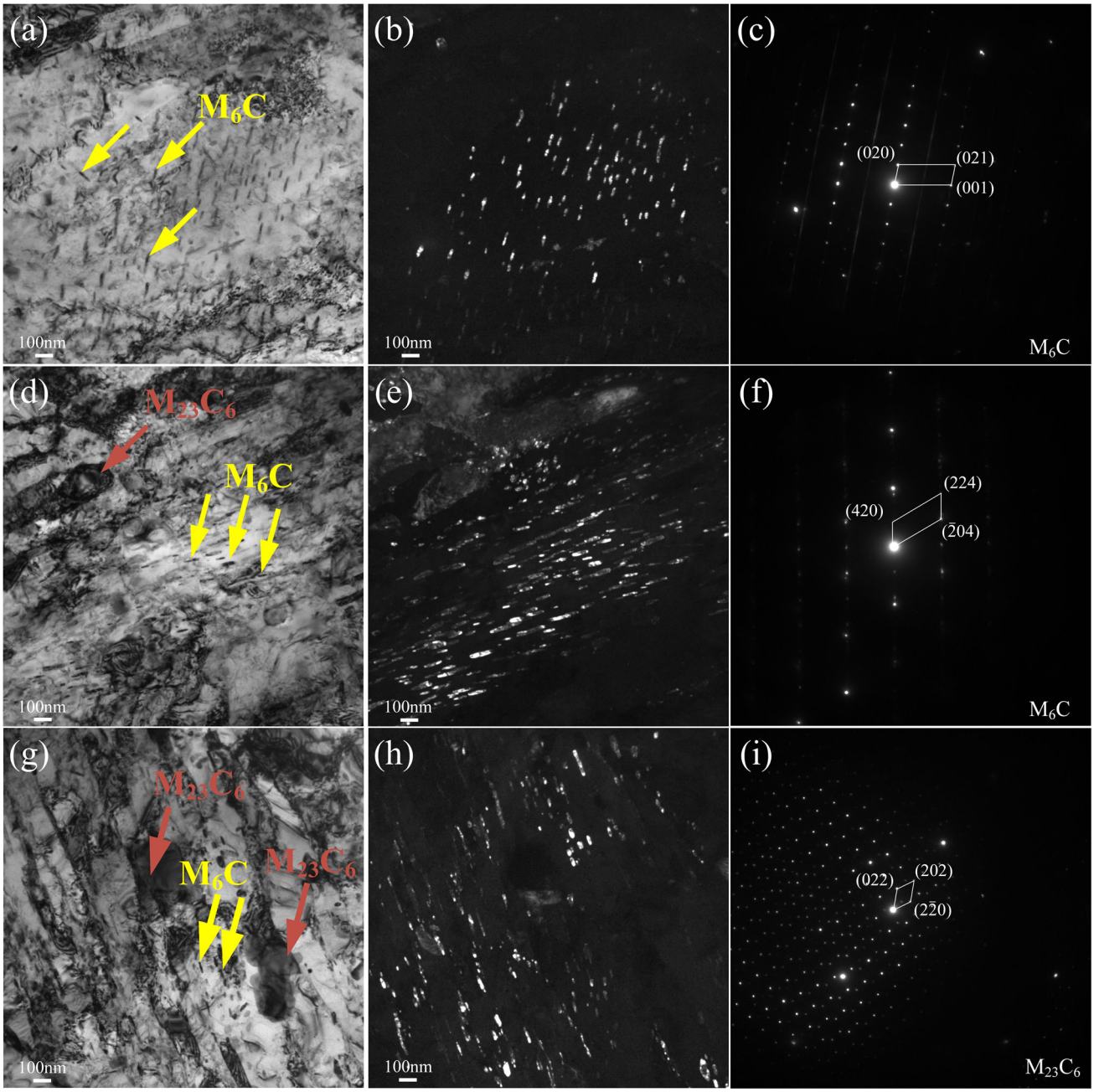

Fig. 8 TEM images and select area electronic diffraction (SAED) patterns of 1.25 Mo (a, b), 2.25 Mo (c, d), and 3.0 Mo (e, f) tempered at 620 °C for 10 h, respectively

Lifshitz-Slyozov-Wagner theory, when the Avrami exponent n is approximately 1/3, the coarsening kinetics is controlled by volume diffusion (Ref 38, 39). It was obvious that the coarsening kinetics of solute atoms in these three steels is controlled by volume diffusion during tempering at 620 °C. The results showed that the average precipitation rate and coarsening rate of carbides were the lowest in the 3.0% Mo steel, (n = 0.37).

Moreover, the better thermal stability of 3.0% Mo steel can be partially attributed to the fact that its high content of Mo promotes the transformation of $M_{23}C_6$ carbide to M_6C carbide, as shown in the calculation results by JMatPro in Fig. 2. It was also proved by the experimental results in TEM images, as shown in Fig. 8, that the 1.89% volume fraction of M_6C carbide for the 3.0% Mo steel was significantly higher than that of 1.53% for the 1.25% Mo steel, but lower than that of 2.73% for the 2.25% Mo steel. This was because the transformation of $M_{23}C_6$ carbide into M_6C carbide was not always complete. M_6C carbides were usually covered by $M_{23}C_6$ carbides that were not completely transformed [9], which may be attributed to the deviation of amount of M_6C carbides in 3.0% Mo steel. M_6C was more stable than $M_{23}C_6$ (Ref 40, 41), and some studies indicated that $M_{23}C_6$ transformed into M_6C (Ref 9, 10, 42, 43). As $M_{23}C_6$ carbide grew faster and was easy to coarsen (Ref 9, 10, 43), it was not conducive to improving the tempering stability of die steel. Therefore, the authors hold the opinion that high Mo content promotes the transformation of $M_{23}C_6$ into M_6C carbide and plays an important role in

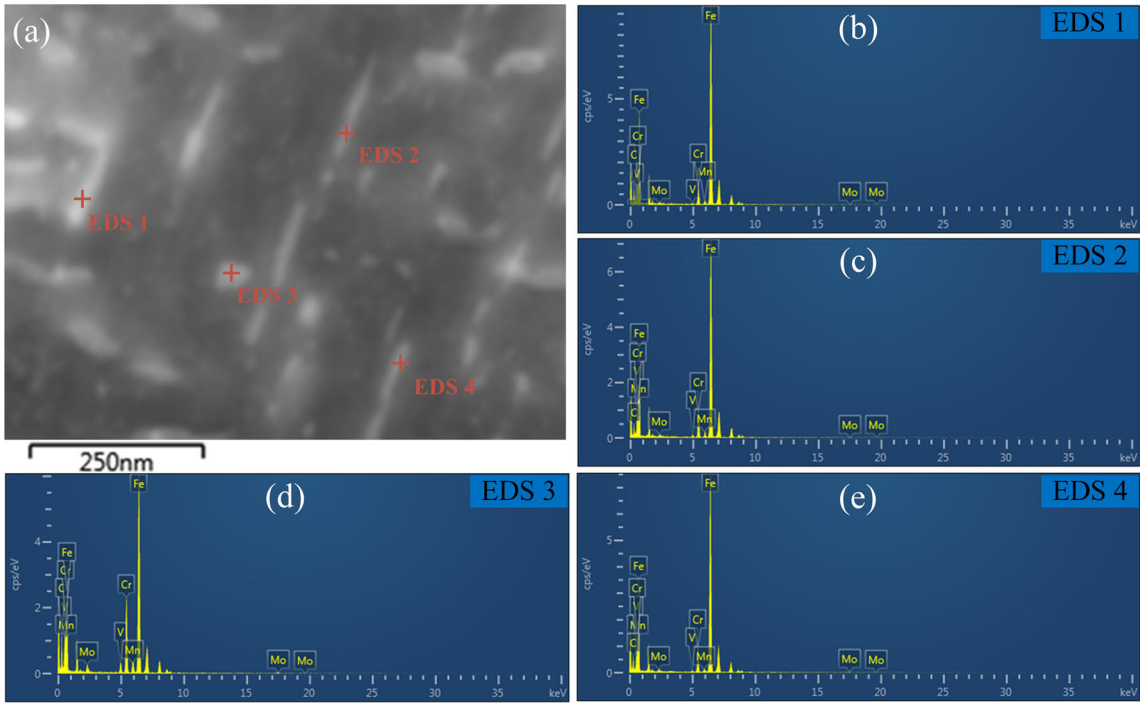

Fig. 9 STEM-EDS data of carbides in 1.25 Mo steel when tempered at 620 °C for 10 h

Table 2 Detailed compositions in atomic percent of Cr, Mo, V, Mn and atomic ratios of Cr/Mo, Cr/V, Cr/Fe, Mo/V, Mo/Fe, and V/Fe of carbides in tempered 1.25Mo steel

Point	Element, at.%					Atomic ratio					
No.	Cr	Mo	V	Mn	Fe	Cr/Mo	Cr/V	Cr/Fe	Mo/V	Mo/Fe	V/Fe
EDS 1	15.71	15.68	2.97	0.74	64.90	1.002	5.290	0.242	5.279	0.242	0.046
EDS 2	5.37	6.29	0.59	0.56	86.69	0.854	9.102	0.062	10.661	0.073	0.007
EDS 3	7.81	8.22	1.02	0.59	82.36	0.950	7.657	0.095	8.059	0.100	0.012
EDS 4	7.24	8.75	0.65	0.23	83.13	0.827	11.138	0.087	13.462	0.105	0.008

improving the hardness of the test steel during the 34 h tempering process.

5. Conclusion

This study investigated the effect of Mo on the microstructure, mechanical properties and thermal stability of 4Cr5Mo2V steels with different Mo content (1.25, 2.25, and 3.0 wt.%). The transformation of carbides and its contributions to mechanical properties and thermal stability at room temperature were discussed. The following conclusions can be drawn from this work:

(1) After being tempered at 620 °C for 10 h, the tensile strength at room temperature of the 1.25, 2.25, and 3.0% Mo steels is 1287, 1347 and 1402 MPa, and the yield strength is 1028, 1080 and 1114 MPa, and the elongation is 23, 26, and 27%, respectively. And the tensile strength at 620 °C of the 1.25, 2.25, and 3.0% Mo steels are 661, 714 and 690 MPa, and the yield strength are 285, 379, and 335 MPa; meanwhile, the elongation is 23, 20, and 22%. As shown from the comparison between steels with high Mo content and low Mo content, the growth of Mo increased the tensile strength and yield strength, while the elongation declined.

(2) With Mo content increasing from 1.25 to 3.0 wt.%, the transition from $M_{23}C_6$ to M_6C was promoted, and the $M_{23}C_6$ carbides decreased gradually. Mo effectively inhibited the nucleation and growth of $M_{23}C_6$. For the reason that the $M_{23}C_6$ carbides are easy to coarsen, it is not conducive to enhancing thermal stability. Therefore, the thermal stability of 4Cr5Mo2V steels increased with the growth of Mo content. It can be concluded that the coarsening kinetics of solute atoms in these three steels was controlled by volume diffusion during tempering at 620 °C. The Avrami exponent n obtained by calculation of the J-M-A equation of the 1.25, 2.25, and 3.0% Mo steels at 620 °C are 0.42, 0.41, and 0.37, respectively.

(3) Through observations by TEM, the dispersed rod-shape carbides were M_6C nano-carbides. The M_6C nano-carbides in the three steels enhance the tensile strengthen

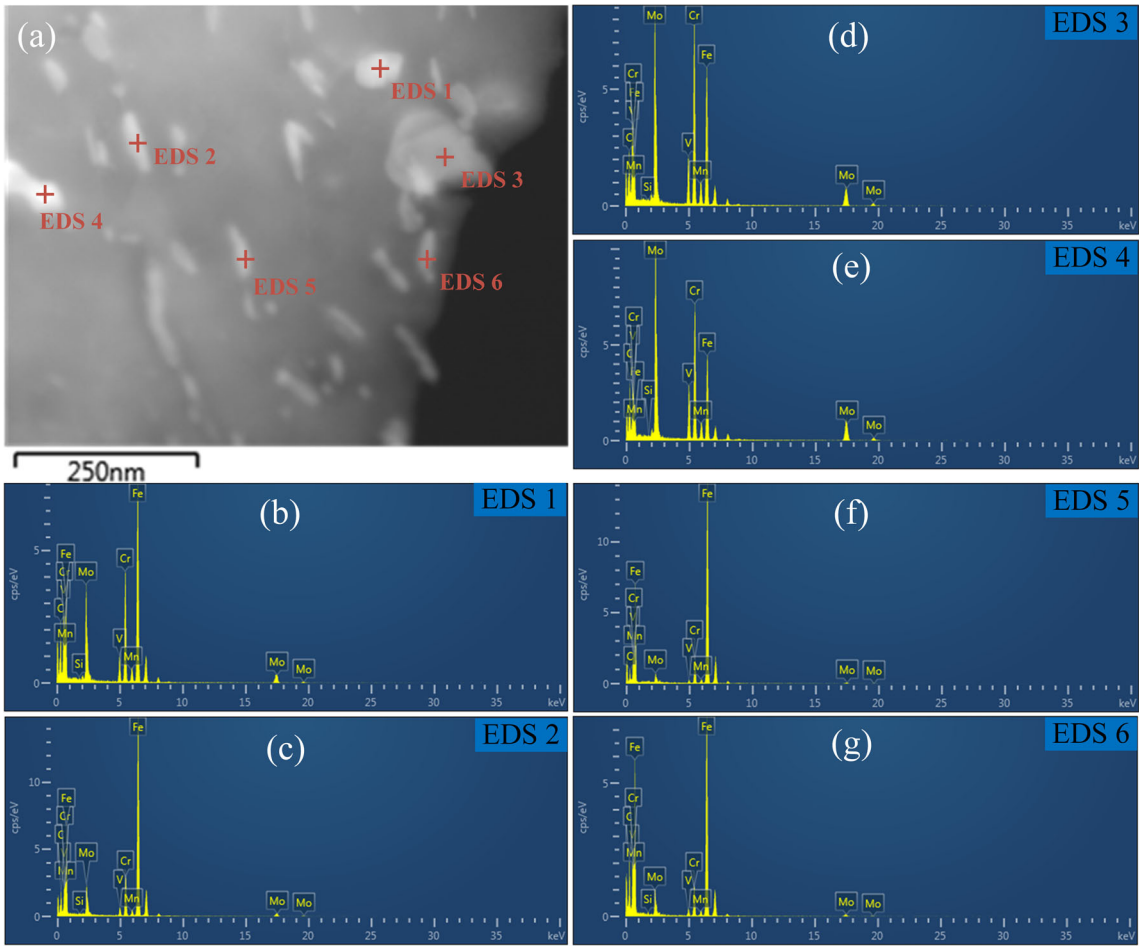

Fig. 10 STEM-EDS data of carbides in 3.0 Mo steel when tempered at 620 °C for 10 h

Table 3 Detailed compositions in atomic percent of Cr, Mo, V, Mn and atomic ratios of Cr/Mo, Cr/V, Cr/Fe, Mo/V, Mo/Fe, and V/Fe of carbides in tempered 3.0Mo steel

Point	Element, at.%					Atomic ratio					
No.	Cr	Mo	V	Mn	Fe	Cr/Mo	Cr/V	Cr/Fe	Mo/V	Mo/Fe	V/Fe
EDS 1	1.81	10.64	0.56	0	2.98	0.170	3.232	0.607	19.000	3.570	0.188
EDS 2	1.50	8.98	0.43	0.04	6.64	0.167	3.488	0.226	20.884	1.352	0.065
EDS 3	3.85	19.14	1.40	0	2.80	0.201	2.750	1.375	13.671	7.975	0.500
EDS 4	2.56	18.12	1.42	0.01	1.48	0.141	1.803	1.730	12.761	12.243	0.959
EDS 5	1.45	6.25	0.26	0.05	11.64	0.232	5.577	0.125	24.038	0.537	0.052
EDS 6	0.46	4.37	0.14	0	2.62	0.105	3.286	0.176	31.214	1.668	0.053

Table 4 The statistic results of nano-carbides parameters in the test alloys

Parameters alloys with different contents of Mo	l_a, nm	d_a, nm	d_{ae}, nm	f, %
1.25% Mo	65.00 ± 1	20.00 ± 1	33.91 ± 1	1.53
2.25% Mo	78.00 ± 1	24.00 ± 1	40.69 ± 1	2.73
3.0% Mo	50.00 ± 1	18.00 ± 1	28.96 ± 1	1.89

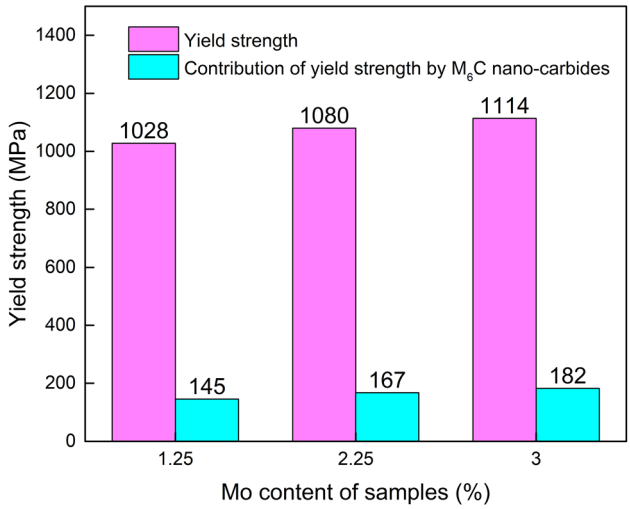

Fig. 11 Contribution of yield strength by the nano-carbides

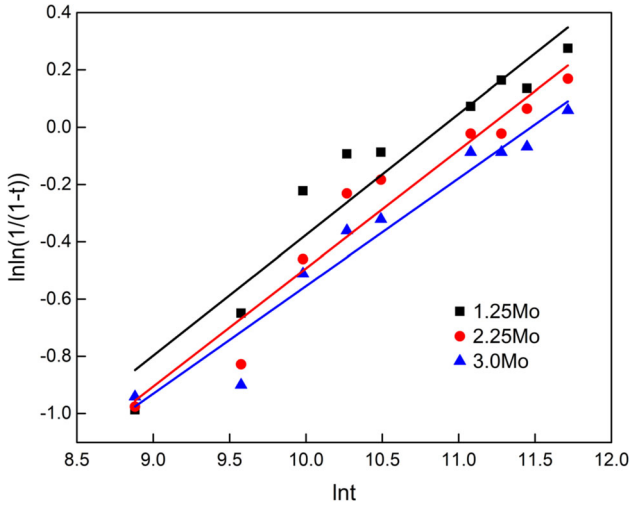

Fig. 12 Avrami exponent n of 1.25, 2.25, and 3.0 Mo steels during tempering at 620 °C

through the Orowan bypass mechanism, providing increment of tensile strength of 145, 167, and 182 MPa, respectively.

Acknowledgment

This research has been supported by the National Key Research and Development Program of China during the 13th Five-year Plan Period (Grant No. SQ2020YFF04012)

References

1. Y.L. Wang, K.X. Song, Y.M. Zhang and G.X. Wang, Microstructure Evolution and Fracture Mechanism of H13 Steel During High Temperature Tensile Deformation, *Mater. Sci. Eng. A*, 2019, **746**, p 127–133.
2. B. Wang, X.F. Zhao, W.Z. Li, M. Qin and J.F. Gu, Effect of Nitrided-Layer Microstructure Control on Wear Behavior of AISI H13 Hot Work Die Steel, *Appl. Surf. Sci.*, 2018, **431**, p 39–43.
3. B. Podgornik, G. Pus, B. Zuzek, V. Leskovsek and M. Godec, Heat Treatment Optimization and Properties Correlation for H11-Type Hot-Work Tool Steel, *Metall. Mater. Trans. A.*, 2018, **49**, p 555–562.
4. D.H. Kim, H.C. Lee, B.M. Kim and K.H. Kim, Estimation of Die Service Life Against Plastic Deformation and Wear During Hot Forging Processes, *J. Mater. Process. Tech.*, 2005, **166**, p 372–380.
5. Q. Zhou, X. Wu, N. Shi, J. Li and M. Na, Microstructure Evolution and Kinetic Analysis of DM Hot-Work Die Steels During Tempering, *Mater. Sci. Eng. A*, 2011, **528**, p 5696–5700.
6. Y. Wang, K. Song and Y. Zhang, High-Temperature Softening Mechanism and Kinetic of 4Cr5MoSiV1 Steel During Tempering, *Mater. Res. Express*, 2019, **6**(9), p 069513.
7. N. Du, H. Liu, P. Fu, H. Liu and D. Li, Microstructural Stability and Softening Resistance of a Novel Hot-Work Die Steel, *Curr. Comput.-Aided Drug Des.*, 2020, **10**, p 238.
8. J. Wang, Z. Xu and X. Lu, Effect of the Quenching and Tempering Temperatures on the Microstructure and Mechanical Properties of H13 Steel, *J. Mater. Eng. Perform.*, 2020, **29**, p 1–3.
9. A. Inoue and T. Masumoto, Carbide Reactions (M3C → M7C3 → M23C6 → M6C) During Tempering of Rapidly Solidified High Carbon Cr-W and Cr-Mo Steels, *Metall. Trans. A*, 1980, **11**, p 739–747.
10. X.B. Hu, M. Zhang and X.C. Wu, Simulations of Coarsening Behavior for m23c6 Carbides in AISI h13 Steel, *J. Mater. Sci. Technol.*, 2006, **22**, p 153–158.
11. J. Zhu, G.T. Lin, Z.H. Zhang and J.X. Xie, The Martensitic Crystallography and Strengthening Mechanisms of Ultra-High Strength Rare Earth Steel, *Mater. Sci. Eng. A*, 2020, **797**, p 140139.
12. A. Liu, L. Wang, L. Pan and X. Cheng, Microstructure and Mechanical Properties of a Novel High-Density Steel Having High Tungsten Content, *Mater. Sci. Eng. A*, 2021, **824**, p 141797.
13. R. Uemori, R. Chijiiwa, H. Tamehiro and H. Morikawa, AP-FIM Study on the Effect of Mo Addition on Microstructure in Ti-Nb Steel, *Appl. Surf. Sci.*, 1994, **76**, p 255–260.
14. W.B. Lee, S.G. Hong, C.G. Park, K.H. Kim and S.H. Park, Influence of Mo on Precipitation Hardening in Hot Rolled HSLA Steels Containing Nb, *Scr. Mater.*, 2000, **43**, p 319–324.
15. B. Kim, C. Celada, D. San Martín, T. Sourmail and P.E.J. Rivera-Díaz-del-Castillo, The Effect of Silicon on the Nano-Precipitation of Cementite, *Acta Mater.*, 2013, **61**, p 6983.
16. G. Miyamoto, J.C. Oh, K. Hono, T. Furuhara and T. Maki, Effect of Partitioning of Mn-Si on the Growth Kinetics of Cementite in Tempered Fe–0.6 Mass% C Martensite, *Acta Mater.*, 2007, **55**, p 5027.
17. D. Rojas, J. Garcia, O. Prat, G. Sauthoff and A.R. Kaysser-Pyzalla, 9%Cr Heat Resistant Steels: Alloy Design, Microstructure Evolution and Creep Response at 650 °C, *Mater. Sci. Eng.*, 2011, **528**, p 5164–5176.
18. D. Wu, F. Wang and J. Cheng, Effects of Nb and Tempering Time on Carbide Precipitations Behavior and Mechanical Properties of Cr-Mo-V Steel for Brake Discs, *Steel Res. Int.*, 2018, **89**, p 1700491.
19. T. Siwecki, J. Eliasson, R. Lagneborg and B. Hutchinson, Vanadium Microalloyed Bainitic Hot Strip Steels, *ISIJ Int.*, 2010, **50**, p 760–767.
20. Z. Wang, W. Hui, Z. Chen, Y. Zhang and X. Zhao, Effect of Vanadium on Microstructure and Mechanical Properties of Bainitic Forging Steel, *Mater. Sci. Eng.*, 2020, **771**, p 138653.
21. J. Sun, S. Wei and S. Lu, Influence of Vanadium Content on the Precipitation Evolution and Mechanical Properties of High-Strength Fe-Cr-Ni-Mo Weld Metal, *Mater. Sci. Eng. A*, 2020, **772**, p 138739-1-138739-S10.
22. R. Wan, S. Feng, L. Zhang and A. Shan, Development and Study of High-Strength Low-Mo Fire-Resistant Steel, *Mater. Des.*, 2012, **36**, p 227–232.
23. S. Jiang, W. Hui, W. Yuan, X. Liu and Z.P. Lu, Ultrastrong Steel via Minimal Lattice Misfit and High-Density Nanoprecipitation, *Sci. Found. China*, 2017, **544**, p 460.
24. Z. Wang, H. Zhang, C. Guo, W.B. Liu, Z.G. Yang, X.J. Sun, Z.Y. Zhang and F.C. Jiang, Effect of Molybdenum Addition on the Precipitation of Carbides in the Austenite Matrix of Titanium Micro-Alloyed Steels, *J. Mater. Sci.*, 2016, **51**, p 4996–5007.
25. W.B. Lee, S.G. Hong, C.G. Park, K.H. Kim and S.H. Park, Carbide Precipitation and High-Temperature Strength of Hot-Rolled High-Strength, Low-Alloy Steels Containing Nb and Mo, *Metall. Mater. Trans. A.*, 2002, **33**, p 1689–1698.
26. K. Zhang, M. Zhang, Z. Guo, N. Chen and Y. Rong, A New Effect of Retained Austenite on Ductility Enhancement in High-Strength

Quenching–Partitioning–Tempering Martensitic Steel, *Mater. Sci. Eng. A*, 2011, **528**, p 8486–8491.
27. Y. Wang, K. Song and Y. Zhang, High-Temperature Softening Mechanism and Kinetic of 4Cr5MoSiV1 Steel During Tempering, *Mater. Res. Express*, 2019, **6**, p 096513.
28. R.C. Thomson and M.K. Miller, Carbide Precipitation in Martensite During the Early Stages of Tempering Cr and Mo-Containing Low Alloy Steels, *Acta Mater.*, 1998, **46**, p 2203–2213.
29. L. Jiang, R. Marceau, B. Guan, T. Dorin and N. Stanford, The Effect of Molybdenum on Clustering and Precipitation Behaviour of Strip-Cast Steels Containing Niobium, *Materialia*, 2019, **8**, p 100462–100462.
30. Z. Wang, H. Zhao, L. Chen, G. Wu and M. Wang, Evolution and its Stability of M23(C, N) 6 Carbonitride in Martensite Ferritic Steel During Long-Term Thermal Aging, *Mater. Charact.*, 2019, **152**, p 36–43.
31. Z. Wang, L. Hui, S. Qin, W. Liu and Z. Wang, Nano-Precipitates Evolution and Their Effects on Mechanical Properties of 17–4 Precipitation-Hardening Stainless Steel, *Acta Mater.*, 2018, **156**, p 158–171.
32. B.B. Zhang, F.K. Yan, M.J. Zhao, N.R. Tao and K. Lu, Combined Strengthening from Nanotwins and Nanoprecipitates in an Iron-Based Superalloy, *Acta Mater.*, 2018, **151**, p 310–320.
33. Z.J. Zhang, J.S. Zhang, Y. Lian, M.Y. Ma, C. Zhao, H.Y. Ye, G.J. Li, C. Zhang and J.F. Huang, Effects of Vanadium Content on the Carbides Transformation and Strengthening Mechanism of MPS700V Hot-Work Die Steel at Room and Elevated Temperatures, *Mater. Sci. Eng. A*, 2021, **813**, p 141091.
34. H.Y. Yue, H. Peng, Y.J. Su, X.P. Wang and Y.Y. Chen, Microstructure and High-Temperature Tensile Property of TiAl Alloy Produced by Selective Electron Beam Melting, *Rare Met.*, 2021, **6**, p 1–10.
35. F. Krumphals, B. Reggiani, L. Donati, T. Wlanis and C. Sommitsch, Deformation Behaviour of a Ferritic Hot-Work Tool Steel with Respect to the Microstructure, *Comput. Mater. Sci.*, 2012, **52**, p 40–45.
36. M. Madivala, A. Schwedt, S.L. Wong, F. Roters, U. Prahl and W. Bleck, Temperature Dependent Strain Hardening and Fracture Behavior of TWIP Steel, *Int. J. Plast.*, 2018, **80**, p 103.
37. B. Mintz, S. Yue and J. Jonas, Hot Ductility of Steels and its Relationship to the Problem of Transverse Cracking During Continuous Casting, *Int. Mater. Rev.*, 1991, **36**, p 187–217.
38. I.M. Lifshitz and V. Slyozov, The Kinetics of Precipitation from Supersaturated Solid Solutions, *J. Phys. Chem. Solids*, 1961, **19**, p 35–50.
39. C. Wagner, Theorie der Alterung von Niederschlägen Durch Umlösen, Zeitschrift für Elektrochemie, Berichte der Bunsengesellschaft für Physikalische, *Chemie*, 2015, **65**, p 581–591.
40. S. Xiang, R.M. Wu, W. Li, T. Hu and S. Huang, Improved Red Hardness and Toughness of Hot Work Die Steel through Tungsten Alloying, *J. Mater. Eng. Perform.*, 2021, **30**, p 7.
41. R.M. Wu, W. Li, M. Chen, S. Huang and T. Hu, Improved Mechanical Properties by Nanosize Tungsten-Molybdenum Carbides in Tungsten Containing Hot Work Die Steels, *Mater. Sci. Eng. A*, 2021, **812**, p 141140.
42. X. Hu, L. Li and X. Wu, Coarsening Behavior of M23C6 Carbides After Ageing Or Thermal Fatigue in AISI H13 Steel with Niobium, *Int. J. Fatigue*, 2006, **28**, p 175–182.
43. D. Nadezhda and K. Rustam, On the Precipitation Sequence in a 10%Cr Steel under Tempering, *ISIJ Int.*, 2011, **51**, p 826–831.